JOURNAL OF MATERIALS SCIENCE 29 (1994) 3517–3526

Cyclic fatigue of hot isostatically pressed silicon nitride at elevated temperatures

C.-K. J. LIN*, M. G. JENKINS†, M. K. FERBER
Metals and Ceramics Division, Oak Ridge National Laboratory, Oak Ridge, Tennessee 37831-6064, USA

Cyclic fatigue properties of a hot isostatically pressed silicon nitride were investigated at 1150, 1260 and 1370 °C in ambient air. The uniaxial tensile tests were conducted under various cyclic loading wave forms and frequencies. The correlation of stress–life relations between cyclic and static fatigue results was evaluated. At 1150–1370 °C, cyclic loading caused less damage than static loading, as evidenced by the longer failure time under cyclic loading versus static loading with the same maximum applied stresses. The cyclic loading effect was more pronounced in high frequency tests at 1260 and 1370 °C and might be related to the viscoelastic behaviour of the intergranular phase. Microstructural analyses and macroscopic cyclic stress–strain and strain–time relations indicated that cyclic loading/unloading may inhibit the normal accumulation of creep damage.

1. Introduction

Silicon nitride ceramics have been the prime candidate materials for advanced heat engine components, because of their high specific strength and good thermal shock resistance [1, 2]. Designs with successful long-term performance require comprehensive characterization of the mechanical and thermal properties in these materials under various modes of loading at elevated temperatures, where fatigue and creep resistances are major concerns. Although the static fatigue and creep rupture behaviour of silicon nitride have been the subjects of numerous studies [3–7], limited work has focused on the elevated-temperature cyclic fatigue properties of silicon nitride, and even less has been related to recently developed hot isostatically pressed (HIPed) silicon nitride ceramics.

Recent studies on the elevated-temperature cyclic fatigue behaviour in Si_3N_4, SiC, Al_2O_3, and Al_2O_3–SiC composite, have demonstrated two distinct observations: (1) cyclic loading at elevated temperatures was found to generate less damage than static loading with the same maximum stress or stress intensity factor [8–16]; (2) cyclic fatigue was essentially a cyclic manifestation of static fatigue, as the cyclic fatigue life or crack growth rate could be rationalized on the basis of the static loading data [12–18]. It has been suggested by Lin *et al.* [12, 13] that the two separate conclusions noted above might be attributed to the difference in cyclic loading paths, in particular the cycle frequency or cycle shape. Cyclic loading with a high frequency or a short hold-time at maximum stress causes less damage than static loading, while no true cyclic loading effect exists for cyclic loading with a lower frequency or a longer hold time at maximum stress. It is therefore implied that cyclic loading would not cause as much damage as static loading in ceramics at elevated temperatures. In contrast, some of the room-temperature fatigue studies [19–23] indicated that cyclic loading effects would degrade strength more than static loading in ceramics.

Previous studies by the authors have focused on the creep, static fatigue (stress–rupture tests) [7], and dynamic fatigue (monotonic stress rate tests) [24] behaviour of a commercially available HIPed silicon nitride at 1150, 1260 and 1370 °C. The objective of the present work was to evaluate the tensile cyclic fatigue behaviour of the HIPed silicon nitride at the same three temperatures using two frequencies and three loading wave forms. A direct comparison of cyclic and static fatigue results was used to provide insights into the effects of loading mode on failure mechanisms.

2. Materials and experimental procedure

Test specimens were fabricated from a commercial HIPed silicon nitride designated as PY6 (GTE Laboratories, Waltham, Massachusetts, 1989–1990 vintage) which contained ~ 6 wt % yttrium oxide as the sintering aid. The typical microstructure of this material contained 1–6-μm-long acicular β-silicon nitride grains surrounded by nominally equiaxed β-silicon nitride grains 0.1–1 μm in diameter. The secondary phases at the two-grain boundaries were in the form of relatively thin layers of an amorphous yttrium silicate. The intergranular phases in the triple-point grain junctions were present as a crystalline yttrium silicate.

Uniaxial tension was employed for all the cyclic fatigue tests carried out at 1150, 1260 and 1370 °C in ambient air. The button-head tensile specimen had a

* *Present address*: Department of Mechanical Engineering, National Central University, Chung-Li 32054, Taiwan.
† *Present address*: Department of Mechanical Engineering, University of Washington, Seattle, Washington 98195, USA.

uniform guage length of 35 mm and guage diameter of 6.35 mm. The low-frequency (0.1 Hz) tests were conducted on commercial closed-loop electromechanical test machines under electronic load control, and the high-frequency (10 Hz) tests were performed on a commercial closed-loop servo-hydraulic test machine. Bending moments were minimized by either self-contained, hydraulic couplers or an adjustable, fixed-grip system attached to water-cooled specimen grips. In all cases, bending at the anticipated maximum cyclic stresses was $\leqslant$ 3% of the axial strain. Compact two-zone resistance-heated furnaces were used to heat the specimens in ambient air environments. Strain measurements were made with direct-contact extensometers employing remote capacitance sensors. Additional details of the testing arrangements are given in [7].

In order to examine the effects of frequency, cycle shape and hold time at maximum stress on the cyclic fatigue behaviour, cyclic fatigue tests were conducted under load control at a constant stress ratio $R = 0.1$ (R = minimum stress/maximum stress) with three wave forms (Fig. 1): (1) symmetric trapezoidal wave at 0.1 Hz (0.5 s ramp and 4.5 s dwell); (2) sinusoidal wave at 10 Hz; (3) triangular wave at 0.1 Hz. The first two wave forms were applied to tests at 1150, 1260 and 1370 °C. Initially, strain was recorded only at discrete intervals for cyclic fatigue tests, with 0.1 Hz trapezoidal loading, due to the uncertainty of whether the movement of extensometer probe tips would generate any surface damage on the specimen and wear in the pivot points of extensometer during continuous cyclic loading. No strain measurement was taken for the tests with 10 Hz sinusoidal loading, due to the frequency limitation for operation of the contact extensometers. Only limited tests were performed with 0.1 Hz triangular loading at 1260 and 1370 °C where strain was monitored continuously to provide information about the evolution of macroscopic deformation under cyclic loading conditions. In these cases, no failures were found to be associated with extensometer contact. Post-failure fractographic analyses were performed with scanning electron microscopy (SEM).

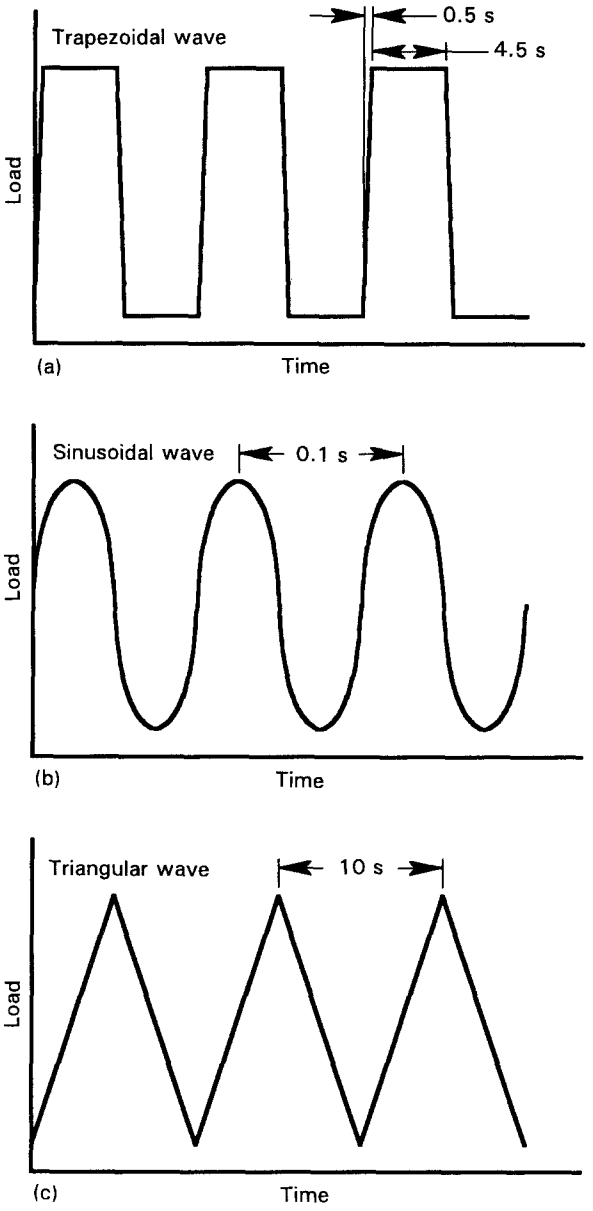

Figure 1 Schematic representation of loading paths for cyclic fatigue tests with a stress ratio $R = 0.1$. (a) Trapezoidal wave form (0.1 Hz, 0.5 s ramp and 4.5 s dwell); (b) sinusoidal wave form (10 Hz); (c) triangular wave form (0.1 Hz).

3. Results and discussion

3.1. Stress–life relations for cyclic fatigue

Fig. 2a–c shows log–log plots of maximum stress against time to failure for cyclic fatigue tests at 1150, 1260 and 1370 °C, respectively. In these plots, each data point represents a single specimen tested to failure. Arrows indicate that failure did not occur when the tests were terminated. The time-delayed fracture behaviour in cyclic fatigue was apparent, as the time to failure for each cyclic wave form increased with decreasing stress level. At 1150 °C, no significant difference in time to failure between trapezoidal and sinusoidal wave forms under the same maximum stress was observed. However, at 1260 and 1370 °C, the time to failure under the same maximum stress in various cyclic loadings takes the following order: sinusoidal > trapezoidal > triangular wave form. These results suggest that the cycle–shape dependence of the cyclic fatigue life for this HIPed silicon nitride at 1150–1370 °C increases with increasing temperature. The above comparison did not demonstrate whether the high-temperature cyclic fatigue behaviour for this material is time-dependent, because the cycle shape is different among selected loading wave forms. In the following section, a slow crack growth (SCG) model is applied to provide the first approximation of whether a true cyclic loading effect exists.

3.2. Correlation of stress–life relations between cyclic and static fatigue

In conventional ceramic fatigue analysis, a SCG model (with a power-law relationship between crack growth rate and stress intensity factor) is widely used for estimating fatigue life. With the assumption that all fatigue failures occur from growth of the initial flaws to final, critical sizes, the following relations can be

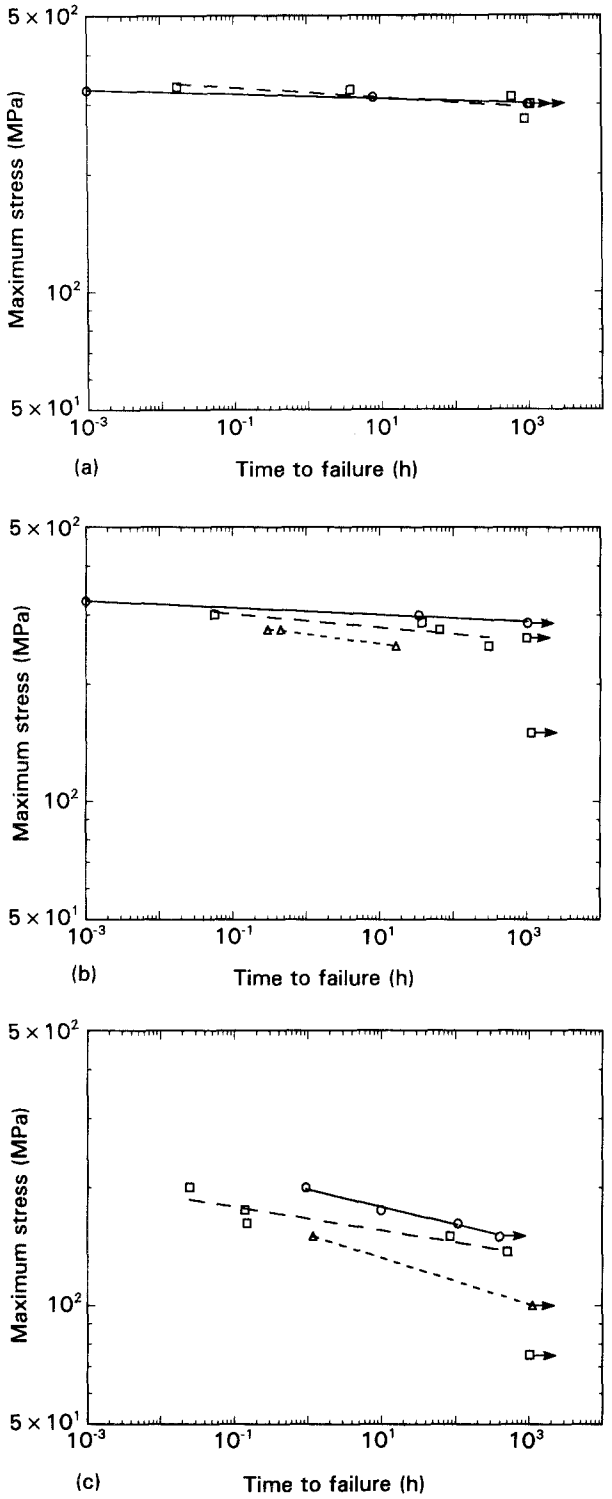

Figure 2 Cyclic fatigue life of PY6 silicon nitride under various frequencies and wave forms at (a) 1150, (b) 1260 and (c) 1370 °C. $R = 0.1$; ○, sinusoidal (10 Hz); □, trapezoidal (0.1 Hz); △, triangular (0.1 Hz).

obtained for uniform stress tests:

$$t_{sf} = \beta\sigma_s^{-N} \quad (1)$$

$$t_{cf} = \beta\sigma_{max}^{-N}\tau\{\int_0^{\tau}[f(t)]^N dt\}^{-1} \quad (2)$$

In Equation 1, t_{sf} is the time to failure for static fatigue under a constant stress, σ_s, β is a constant related to initial flaw size and geometry, and N is the crack growth exponent. Time to failure in cyclic fatigue, t_{cf}, is given in Equation 2 where σ_{max} is the maximum stress, τ is the cycle period, and $f(t)$ is a function of time associated with the cyclic wave form such that the applied stress in a cycle can be described as $\sigma(t) = \sigma_{max}f(t)$. Details of the derivation of Equations 1 and 2 are given in [25–27]. Based on the stress–life relations in Equations 1 and 2, a so-called 'effective' time approach is used to correlate static and cyclic fatigue behaviour. The effective time to failure for static fatigue is equal to the actual time to failure, t_{sf}. However, the effective time to failure for cyclic fatigue is equal to the actual time to failure reduced by a factor, because only a portion of the loading cycle is spent at the maximum stress in cyclic fatigue testing. The effective time to failure for cyclic fatigue can be defined as follows:

$$t_{cf,\,eff} = t_{cf}\tau^{-1}\{\int_0^{\tau}[f(t)]^N dt\} \quad (3)$$

Thus for equivalent values of σ_{max} and σ_s, the effective time to failure in cyclic fatigue is equal to the failure time in static fatigue, provided that slow crack growth of similar initial flaws is the primary mechanism for all the failures. Therefore, making comparisons among the effective times to failure in static and cyclic fatigue under similar maximum stresses will aid in assessing whether all fatigue failures are dominated by the same slow crack growth mechanism. With the results of such a comparison, one can obtain the first approximation as to whether there exists any cyclic loading effect on the failure mechanism.

The values of N were obtained from the stress–life relation in static fatigue (Equation 1) through a power–law curve fit. Results of static fatigue tests [7] provided estimates of N as 22 at 1150 °C, and 6.4 at 1260 and 1370 °C. These N values were then applied to Equation 3 to convert the actual failure time into effective time to failure in cyclic fatigue. Cyclic and static fatigue results are compared in log–log plots of maximum stress against effective time to failure (Fig. 3). The comparison indicates that the levels of maximum applied stress required to generate failures within 1 to 1000 h were greater in cyclic fatigue tests (both low and high frequency) than those in static fatigue tests. In this region, the effective failure times under cyclic loading were longer than those under static loading with the same maximum applied stresses. This difference in failure times becomes greater when the comparison is made by using the actual cyclic fatigue failure times.

As shown in Fig. 3a–c, the difference between static and cyclic fatigue life decreases with increasing stress level. Although a direct comparison could not be made at high applied stresses (failure time less than 1 h) due to the absence of static fatigue data, both static and cyclic fatigue failures, at stress levels near the fast fracture strength, would result from slow crack growth of a dominant inherent flaw. Such a transition of dominant failure mechanism from creep rupture to SCG in static fatigue at elevated temperatures has been shown in other silicon nitrides [3, 4]. Consequently, the cyclic effective life would be closer to the static fatigue life at higher stresses, which is somewhat consistent with the SCG model approach. However, for stresses well below the fast fracture strength, the

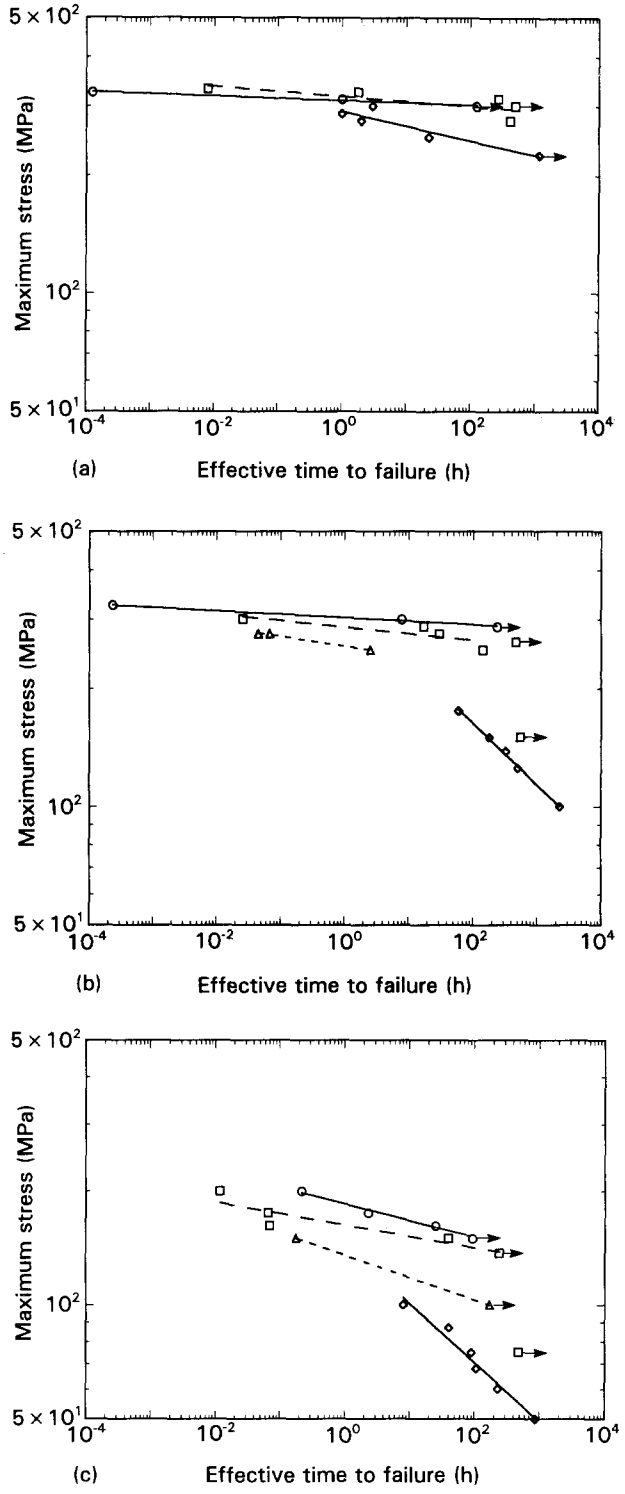

Figure 3 Comparison of static and cyclic fatigue life by an effective time to failure approach for data generated at (a) 1150, (b) 1260 and (c) 1370 °C. ○, sinusoidal (10 Hz); □, trapezoidal (0.1 Hz); △, triangular (0.1 Hz); ◇, static loading.

static and cyclic fatigue life could not be well correlated by the SCG model, suggesting a true cyclic loading effect. More importantly, the evolution of damage under cyclic loading was much less than for static loading. Such behaviour at elevated temperatures is opposite to the room-temperature fatigue behaviour of some ceramics, where cyclic loading has a more deleterious effect on resistance to fracture than static loading [19–23]. This difference is attributed, at least in part, to the softening of the intergranular phase at elevated temperatures, where the mechanisms responsible for the detrimental cyclic loading effect at room temperature become ineffective [16].

Fig. 3 also indicates that under the same maximum applied stress, the effective cyclic fatigue life for specimens tested at 1260 and 1370 °C still takes the following order: sinusoidal > trapezoidal > triangular wave form. This difference in effective cyclic fatigue life between low- and high-frequency tests could be as large as an order of magnitude or more, depending on the applied stress levels. This result implies that cyclic fatigue life for this PY6 silicon nitride at 1260 and 1370 °C is cycle-shape or stress-rate dependent. Note the maximum stress rates are at the orders of 10^1, 10^2 and 10^3 MPa s^{-1} for triangular, trapezoidal and sinusoidal loading, respectively. Such dependence of cyclic fatigue life on cycle shape or stress rate might be related to the rate-sensitivity of the viscous characteristics of the secondary phase. Apparently, higher frequency or higher stress rate would cause less strength degradation. Similar frequency and cycle-shape effects were also present in other ceramics at elevated temperatures [12–15].

The influence of stress rate on the elevated-temperature damage mechanisms for the PY6 material has been discussed elsewhere [24]. The static fatigue failure mechanisms agree with the dynamic fatigue failure mechanisms if the stress rates in static fatigue tests are considered extremely low. At 1150 °C, SCG has been reported as the dominant failure mechanism for static fatigue [7], which agrees with the fact that SCG was responsible for all the dynamic fatigue failures regardless of the levels of stress rate. At 1260 and 1370 °C, static fatigue failures were found to be dominated by creep rupture [7] which also controlled the dynamic fatigue failures at low stress rates ($\leqslant 10^{-2}$ MPa s^{-1}). The absence of extensive creep damage at 1150 °C in both static and dynamic fatigue was a consequence of the increased viscosity of the intergranular phase [7, 24]. The stress rates in cyclic fatigue tests were so high that their failure mechanisms were different from those in static fatigue, particularly at 1260 and 1370 °C, as supported by the dynamic fatigue results.

The apparent N values (> 80 at 1150 °C, > 40 at 1260 °C, and > 23 at 1370 °C) in cyclic fatigue are much greater than those in static fatigue, suggesting the failure mechanisms are different between static and cyclic fatigue. The N values estimated from dynamic fatigue data [24] were 98 for all applied stress rates at 1150 °C, 24 and 7.1 for stress rates $> 10^{-2}$ MPa s^{-1} at 1260 and 1370 °C, respectively, and 18 and 3.9 for stress rates $\leqslant 10^{-2}$ MPa s^{-1} at 1260 and 1370 °C, respectively. Except at 1150 °C, where the N values of cyclic and dynamic fatigue are comparable, the N values of cyclic fatigue at 1260 and 1370 °C are also greater than those in the SCG regime (stress rates $> 10^{-2}$ MPa s^{-1}) of dynamic fatigue at 1260 and 1370 °C. The differences in N values imply that the failure mechanisms and/or crack growth mechanisms for cyclic loading and monotonic loading (including static loading and constant stress rate loading) are not identical.

The loading/unloading in the cyclic fatigue tests appeared to inhibit the creep damage nucleation and accumulation process, in particular at 1260 and 1370 °C, and decrease the crack growth rates, thus allowing greater stresses to be sustained for similar failure times. This is supported by the cyclic stress–strain and strain–time behaviour which will be discussed below.

3.3. Cyclic stress–strain behaviour

As described previously, only discrete cyclic stress–strain behaviour was recorded for tests under 0.1 Hz trapezoidal loading at 1150, 1260 and 1370 °C. The typical cyclic stress–strain behaviour for these cases is shown in Fig. 4. For all applied stress levels at 1150–1370 °C, the cyclic stress–strain behaviour remained linear to the final few cycles prior to the failure of specimens. Moreover, the Young's modulus, slopes of the cyclic stress–strain curves, did not change significantly during cyclic fatigue testing. Previous studies [24, 28–30] have indicated that damage accumulation by formation and growth of creep cavities and microcracks could cause a progressive decrease in Young's modulus and lead to an apparent non-linear stress–strain relation. Therefore the absence of measurable hysteresis in the cyclic stress–strain response implies that little, if any, creep cavitation or microcracking occurred during cyclic fatigue testing under 0.1 Hz trapezoidal loading. This is supported by the monotonic tensile stress–strain behaviour in dynamic fatigue tests [24]. At 1260 and 1370 °C, non-linear stress–strain behaviour prevailed at stress rate $\leqslant 10^{-2}$ MPa s^{-1} where creep rupture was the dominant failure mechanism. When the stress rates became greater than 10^{-2} MPa s^{-1} at 1260 and 1370 °C, the stress–strain response became linear and SCG was the governing failure mechanism. At 1150 °C, the tensile

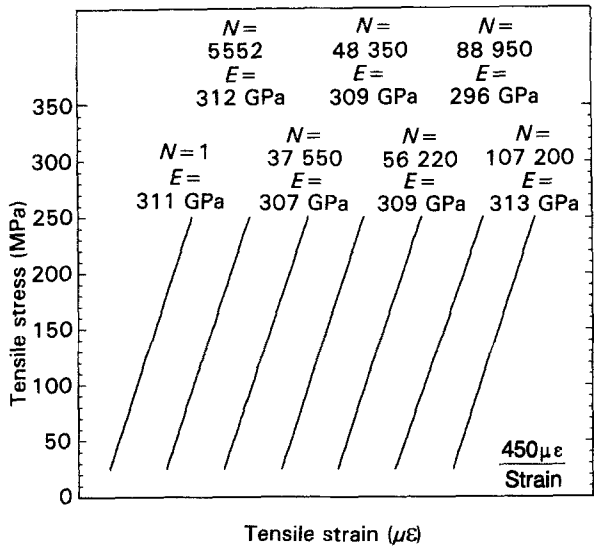

Figure 4 Cyclic stress–strain behaviour of PY6 silicon nitride tested under 0.1 Hz trapezoidal loading at 1260 °C with stress of 25–250 MPa. N_f = 110 110 cycles. Note these cyclic stress–strain curves were discretely recorded without monitoring the strain–time relation for the entire test, such that only a relative scale instead of an absolute scale was used for the abscissa.

stress–strain curves under all stress rates (from 10^{-4} to 37 MPa s^{-1}) exhibited linear behaviour (with nearly identical slopes) and SCG was the prevailing failure mechanism.

Although a hold-time at maximum stress was applied in each cycle during the 0.1 Hz trapezoidal loading, no measurable strain increment was observed during the stay at maximum stress. Apparently, the hold-time at maximum stress is shorter than the characteristic time constant for the rate sensitivity of deformation of the viscous intergranular phase, and no significant creep strain is generated. If the hold-time at maximum stress or the cycle period is comparable with such a characteristic time constant, the true cyclic loading effect might disappear and prediction of the cyclic fatigue life from the static fatigue data might become possible [12–15]. This characteristic time constant is dependent on the viscosity of the intergranular phase and the elastic modulus of the material. Based on the results of a previous study [31], this characteristic time for PY6 silicon nitride is expected to exceed 24 h at 1370 °C, and more importantly, unloading is expected to play a major role in extending the fatigue life. In that study [31], a limited number of static fatigue tests were performed at 1370 °C with application of a short unload/reload cycle every 24 h for the purpose of measuring the variation of Young's modulus with creep damage evolution. The static fatigue life was substantially increased by this cycling over that measured under 'no cycle' conditions, even though only tens of cycles were applied throughout the nearly static loading tests. A less pronounced tertiary regime in the strain–time curves and much lower cavity density were observed for those static fatigue specimens tested with interruption of an unload/load cycle every 24 h. This suggests that cyclic fatigue–creep interactions did not occur in the PY6 silicon nitride at elevated temperatures. It is likely that viscoelastic strain recovery, and/or stress relaxation occurring during the initial unloading, effectively reduced the driving force for subsequent cavitation.

As creep rupture was the controlling failure mechanism for static fatigue at 1260 and 1370 °C, a limited number of cyclic fatigue tests were conducted under 0.1 Hz triangular loading at 1260 and 1370 °C with the extensometers in continuous contact with the specimens for the entire tests. In these tests, not only the cyclic stress–strain response but also the strain–time history was obtained. Similar to the results generated at 0.1 Hz trapezoidal loading, the cyclic stress–strain behaviour obtained under 0.1 Hz triangular loading was also free of hysteresis and remained linear to the final few cycles before failure. Such similarity in cyclic stress–strain response between trapezoidal and triangular loading suggests that the loading/unloading procedure in cyclic fatigue tests appears to inhibit the nucleation and/or growth of creep cavities and microcracks, no matter what wave form is applied.

Fig. 5 shows the typical strain–time plot for a cyclic fatigue test (0.1 Hz triangular loading with a maximum stress of 100 MPa) compared to strain–time histories of static fatigue tests at 1370 °C. The strain–time curve plotted in Fig. 5 for the cyclic

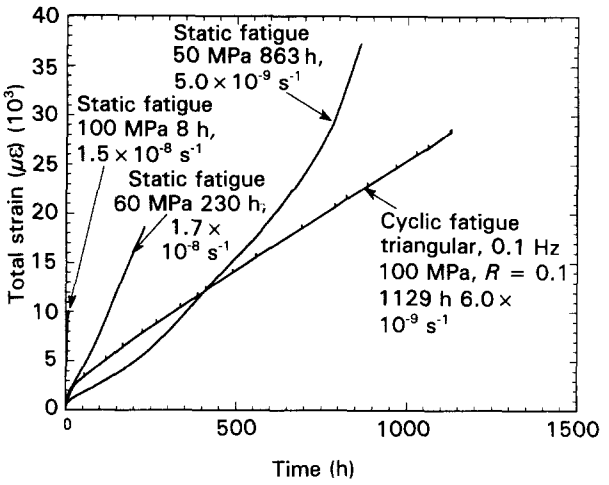

Figure 5 Comparison of strain–time relations for static and cyclic fatigue of PY6 silicon nitride at 1370 °C. The label for each curve includes the applied maximum stress, failure time, and minimum strain rate. Each of the 'vertical' segments on the cyclic fatigue curve represents the corresponding cyclic stress–strain response at that particular time.

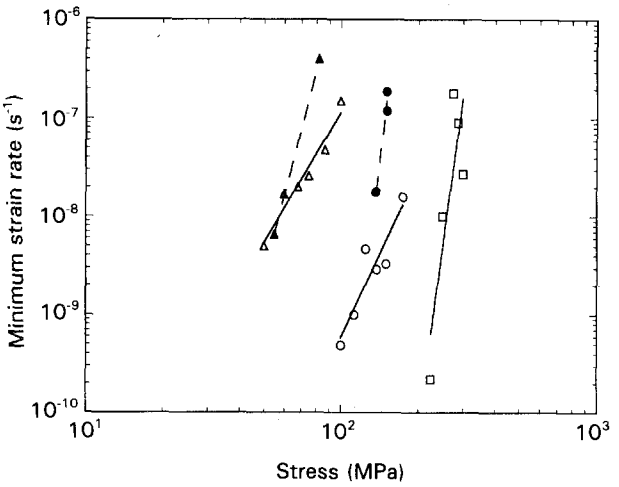

Figure 6 Comparison of minimum strain rate for static and cyclic fatigue of PY6 silicon nitride at 1150–1370 °C as a function of static or mean stress. T = □, 1150; ○, ●, 1260; △, ▲, 1370 °C. Open symbols, static fatigue; closed symbols, cyclic fatigue.

fatigue test was taken at the minimum stress level with additional short discrete 'vertical' segments which represent the cyclic stress–strain response at that particular time. The upper peak of each segment is the corresponding strain at the maximum stress. Since the cyclic stress–strain behaviour was linear throughout almost the entire cyclic fatigue test, using other strain values (e.g. that corresponding to the mean or maximum stress level) as the reference strain in strain–time history would simply translate the strain–time curve along the strain axis, but would not alter its slope. In Fig. 5, the cyclic fatigue strain–time curve shows a pronounced steady-state regime (or minimum strain rate regime) and absence of tertiary regime as compared to the short steady-state regime and dominant tertiary regime in the static fatigue tests. The absence of the tertiary regime provides more evidence for the conclusion that the normal damage accumulation process in static fatigue was interrupted by the loading/unloading steps in cyclic fatigue.

Although stress–strain hysteresis was not observed during cyclic fatigue testing, an extensive amount of strain ratchetting was found (see Fig. 5). Note that strain ratchetting here refers to the time-dependent progression of the cyclic stress–strain curves along the strain axis. Creep deformation under a tensile mean stress was the first speculation as the mechanism responsible for this strain ratchetting. As shown in Fig. 5, at the early stage of the strain–time history, the cyclic fatigue curve (mean stress = 55 MPa) fell between the two static fatigue curves (applied stresses = 50 and 60 MPa, respectively). This seems to agree with the postulation. However, as no tertiary regime occurred under cyclic loading, the cyclic fatigue curve eventually fell below the static fatigue curve with an applied stress of 50 MPa, suggesting the mechanisms controlling the process of damage accumulation for static and cyclic fatigue were different.

More evidence supporting this conclusion is presented in Fig. 6, where minimum strain rate is plotted against applied stress in log–log base for both static and cyclic fatigue (0.1 Hz triangular loading) tests. The minimum strain rate for cyclic fatigue was defined as the minimum degree of increase in the strain corresponding to the minimum stress level throughout the test. The mean stress was used as the abscissa for the cyclic fatigue tests in Fig. 6. Fitting the data given in Fig. 6 to a simple power-law relation between minimum strain rate and applied stress ($\dot{\varepsilon}_{min} = A\sigma^n$, where A is a constant) yields the following n values: n = 19, 5.6, and 4.4 for static fatigue at 1150, 1260 and 1370 °C, respectively, while n = 22 and 10 for cyclic fatigue tests at 1260 and 1370 °C, respectively. The significant difference in the corresponding stress exponent values between static fatigue (n = 5.6 and 4.4) and cyclic fatigue (n = 22 and 10) at 1260 and 1370 °C indicates that the damage mechanisms are different for these two loading histories. Therefore, creep might not be the primary damage mechanism leading to the final failures in cyclic fatigue specimens. The similarity of high n values between static fatigue at 1150 °C (n = 19) and cyclic fatigue at 1260 and 1370 °C (n = 22 and 10, respectively) suggests that a damage accumulation process analogous to SCG might be the primary failure mechanism for cyclic fatigue. Note that the strain–time curves for static fatigue at 1150 °C also had a dominant steady state regime [7]. In this sense, the observed strain ratchetting for cyclic fatigue at 1260 and 1370 °C might actually reflect compliance changes resulting from the subcritical extension of a localized damage zone in a way similar to SCG. More microstructural evidence for this conclusion will be provided in the following section.

Fig. 6 also shows that the minimum strain rates at high applied stress levels were higher under cyclic loading than those under static loading when comparison was made using mean stress for cyclic fatigue. However, if maximum stress is employed for the comparison, the minimum strain rates would be lower in cyclic fatigue compared to static fatigue, which agrees with the stress-life characteristics as described previously. Note that using maximum stress as the

abscissa for cyclic fatigue tests in Fig. 6 would not change the slope (stress exponent) but translate the curves horizontally toward the right along the stress axis. Therefore, in this case, a comparison of stress exponent values might be more useful in examining the identity of failure mechanisms between cyclic and static fatigue.

In Fig. 7, a Monkman–Grant plot [32] ($t_f = C(\dot{\varepsilon}_{min})^{-m}$, where C is a constant) of the minimum strain rate against time to failure indicates distinct curves for each test temperature of 1260 and 1370 °C, regardless of loading history. The values of m estimated from the data in Fig. 7 are approximately 1.5, and relatively independent of temperature. The agreement of cyclic and static fatigue data fitted in the Monkman–Grant relationship implies that stress may not be an appropriate controlling parameter for correlating static and cyclic fatigue life at elevated temperatures. However, this agreement inevitably begs the question that the failure mechanisms in static and cyclic fatigue are different, as described above. More microstructural evidence for the different failure mechanisms in cyclic and static fatigue is given below.

3.4. Microstructural analysis results

Typical fracture surfaces of cyclic specimens tested at 1150, 1260 and 1370 °C are shown in Fig 8a–c, respectively. At 1150 °C, the fracture surfaces contained well-defined mirror, mist, and hackle regions (Fig. 8a). A region of apparent slow crack growth (s) from a pre-existent defect was also identified within the mirror region. All of the cyclic fatigue failures at 1150 °C were related to pre-existent flaws located in the volume or at the surface. Even though both static and cyclic fatigue failures at 1150 °C were due to subcritical crack extension of pre-existent flaws, the comparison of stress–life relations implies that crack propagation rates were less in cyclic loading than in static loading. The lesser damage caused by cyclic fatigue relative to static fatigue in ceramics at elevated temperatures might be related to the viscous intergranular phase

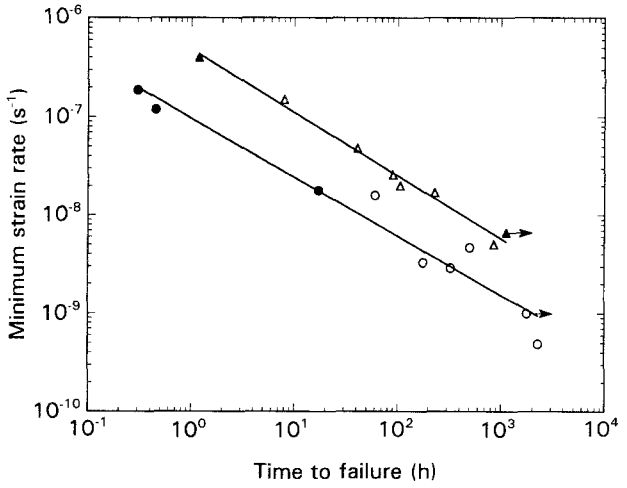

Figure 7 Comparison of Monkman–Grant type relations for static and cyclic fatigue of PY6 silicon nitride at ○, ●, 1260 and △, ▲, 1370 °C. Open symbols, static fatigue; closed symbols, cyclic fatigue.

[8–13]. For example, the effect of bridging the crack surfaces by the viscous intergranular phases could be more pronounced in cyclic loading than in static loading under certain conditions [13]. Because of the inability of the viscous ligaments behind the crack tip to relax during the high-frequency cycling, the effective stress intensity factor at the crack tip is larger under static loading than for cyclic loading, with a high frequency or a short hold time at maximum applied stress. In this sense, the crack growth rate is lower in cyclic loading than in static loading. Lower crack growth rates in cyclic loading than in static loading, with the same maximum applied stress intensity factor at elevated temperatures, have been reported in other ceramics [9, 10].

For cyclic fatigue specimens tested at 1260 °C, the fracture surfaces still showed the mirror-mist-hackle feature with failure originating from the surface. Only a couple of specimens tested at the highest applied stresses clearly showed the internal pre-existent flaws as the fracture origins. The majority of the specimens had surface-initiated failures but no clear fracture origins, such as pre-existent defects, could be identified (Fig. 8b). A possible explanation for this phenomenon is that at temperatures $\geqslant$ 1260 °C, the oxidation rate increased as evidenced by the outer darker rings on the fracture surfaces shown in Fig 8b and c, thereby providing preferred sites for fracture initiation. As observed in other silicon nitrides [33, 34], oxidation could increase the strength by rounding or blunting pre-existent flaws or decrease the strength by producing new flaws such as bubbles, pits, and microcracks in the oxide scale. The effects of the oxidation process and products on the mechanical properties are related to complex factors such as impurities and sintering aids, temperature, duration of oxidation, loading conditions during oxidation, and others [33, 34]. It is probably due to the oxidation that most of the cyclic fatigue failures at 1260 °C were initiated at or near the surfaces and their origins could not be clearly identified.

The features for the fracture surfaces of cyclic fatigue specimens tested at 1370 °C appear similar to those generated at 1260 °C, except that the mirror regions are larger due to the lower applied stresses (Fig. 8c). In addition, a small damage zone with greater roughness was observed within the mirror region on the fracture surfaces of a few cyclic fatigue specimens tested at 1370 °C. Macroscopically, the feature of this small damage zone does not look like that of the slow crack growth region at 1150 °C, but is similar to the larger creep damage zone previously identified for the static fatigue specimens tested at 1260 and 1370 °C [7]. However, microscopically, no extensive creep cavities were detected throughout the guage sections of cyclic fatigue specimens tested at 1150–1370 °C. This is one of the major differences in the microstructure between the failed static and cyclic fatigue specimens, in particular at 1260 and 1370 °C (see Figs 9a and b). The origin of this small damage zone from the surface once again implies that surface oxidation might make some contribution to the fatigue failures at 1260 and 1370 °C.

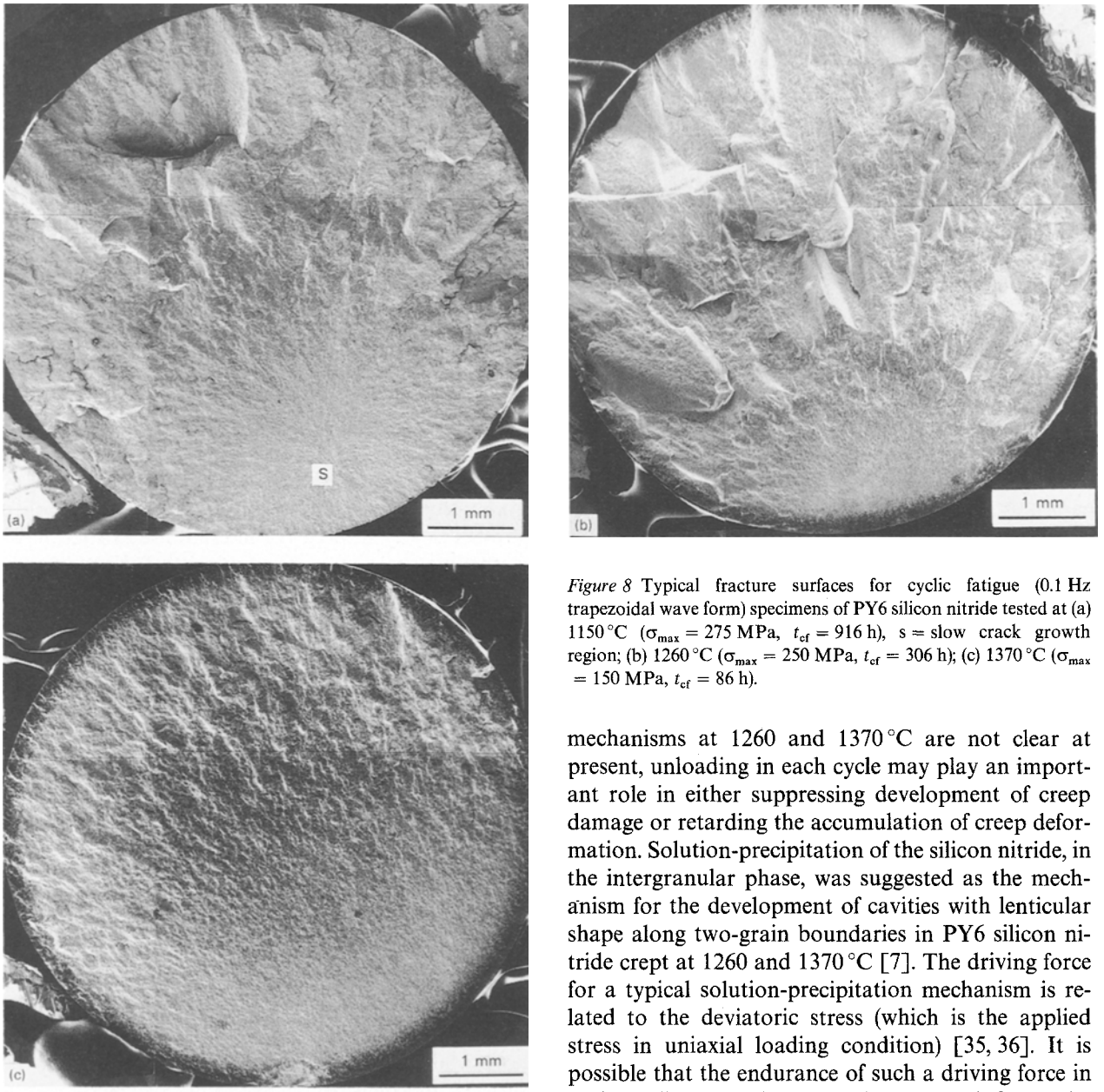

Figure 8 Typical fracture surfaces for cyclic fatigue (0.1 Hz trapezoidal wave form) specimens of PY6 silicon nitride tested at (a) 1150 °C (σ_{max} = 275 MPa, t_{cf} = 916 h), s = slow crack growth region; (b) 1260 °C (σ_{max} = 250 MPa, t_{cf} = 306 h); (c) 1370 °C (σ_{max} = 150 MPa, t_{cf} = 86 h).

Based on these observed features of fracture surfaces and microstructure, it is likely that a damage accumulation process analogous to SCG might be the primary failure mechanism for cyclic fatigue at 1260 and 1370 °C. This damage accumulation process might involve the subcritical extension of a localized damage zone originating from a surface where oxidation-assisted damage or oxidation–modified pre-existent flaws would provide favourable sites for crack nucleation. The difference of microstructural observations in cyclic and static fatigue is consistent with the macroscopic observations that cyclic fatigue data generated at 1260 and 1370 °C demonstrated significantly higher values of crack growth exponent, N, and stress exponent, n, over those generated by static fatigue loading at the same temperatures.

The fact that cyclic fatigue specimens did not display such extensive creep cavities as observed in the static fatigue specimens tested at 1260 and 1370 °C agrees with the characteristics of stress–life and strain–time results. Although the exact cyclic fatigue mechanisms at 1260 and 1370 °C are not clear at present, unloading in each cycle may play an important role in either suppressing development of creep damage or retarding the accumulation of creep deformation. Solution-precipitation of the silicon nitride, in the intergranular phase, was suggested as the mechanism for the development of cavities with lenticular shape along two-grain boundaries in PY6 silicon nitride crept at 1260 and 1370 °C [7]. The driving force for a typical solution-precipitation mechanism is related to the deviatoric stress (which is the applied stress in uniaxial loading condition) [35, 36]. It is possible that the endurance of such a driving force in each loading period was not long enough for nucleation and/or growth of cavities for selected cyclic loading conditions in the present study. This might result from relaxation of local stress concentration at potential sites for cavity development and recovery of viscoelastic deformation during unloading. As mentioned earlier, unloading would also enhance the crack surface bridging effect of the viscous intergranular phase and reduce the crack growth rate in cyclic fatigue loading.

Crystallization of the intergranular glass at elevated temperatures can also influence the creep properties in ceramics. This effect is attributed to changes in the volume fraction and viscosity of the grain-boundary glass [37]. In particular, if creep occurs either by a solution-precipitation process or by viscous flow, then a gradual decrease of the amount of glass accompanied by a continuous increase in viscosity in the interfacial phase will enhance the creep resistance. As a complete devitrification of the interfacial glass was rarely observed in silicon nitrides, this crystallization process will continuously alter the composition of retained interfacial glass during creep [38]. Progressive devitrification of the residual intergranular glass

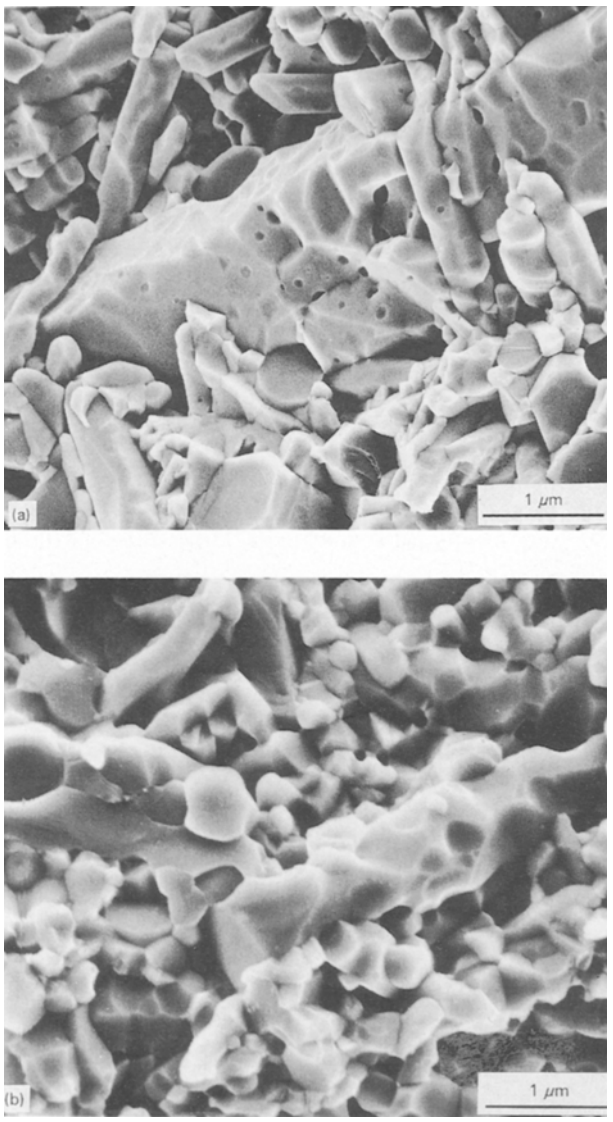

Figure 9 SEM micrographs for static and cyclic fatigue specimens of PY6 silicon nitride tested at 1370 °C. (a) Static fatigue, $\sigma_s = 75$ MPa, $t_{sf} = 90$ h (with cavities along two-grain boundaries); (b) cyclic fatigue, 0.1 Hz trapezoidal loading, $\sigma_{mean} = 75$ MPa ($\sigma_{max} = 137$ MPa), $t_{cf} = 516$ h (without cavities).

is a contributing factor to the long-term transient creep behaviour in other HIPed and sintered silicon nitrides [38, 39]. Although the intergranular phases in the triple-point grain junctions of the as-received PY6 specimens were in a form of crystalline yttrium silicate, the two-grain boundaries were composed of relatively thin layers of an amorphous yttrium silicate. However, the influence of devitrification on the creep properties of PY6 silicon nitride might be a secondary factor as supported by the presence of pronounced steady-state and tertiary behaviour in the strain–time curves of static fatigue results [7]. In order to better quantify possible time-dependent and stress-state-dependent variations in grain boundary crystallography, more systematic experiments and transmission electron microscopy (TEM) analyses are necessary for future work. It is important to understand how and to what extent the devitrification affects the rate of deformation during creep and how the loading mode, in particular cyclic loading, influences the effective response of the intergranular phases in this HIPed silicon nitride.

4. Conclusions

Comparison of stress–life relations between static and cyclic fatigue indicates that cyclic loading provided more extensive time to failure for a selected HIPed silicon nitride at 1150–1370 °C. The tensile static and cyclic fatigue data could not be described by a universal SCG model at temperatures $\geqslant 1150$ °C. Caution is advised in applying the SCG model to predict the stress–life relation for cyclic fatigue based on static fatigue data. This is especially true at elevated temperatures, where mechanisms other than slow crack growth, such as creep processes, viscoelastic effects, and oxidation, may contribute to the final failure.

The lack of measurable hysteresis in cyclic stress–strain behaviour implies that little, if any, creep damage such as cavitation and microcracking was generated during cyclic fatigue testing. In this sense, strain ratchetting observed during cyclic fatigue testing was probably caused by a damage accumulation process analogous to SCG. This conclusion is supported by the greater values of crack growth exponent, N, and stress exponent, n, for cyclic fatigue over those generated by static fatigue at 1260 and 1370 °C where creep rupture was the dominant failure mechanism. Moreover, microstructural analyses provide no evidence of extensive creep cavities in cyclic fatigue specimens.

Cyclic loading of selected HIPed silicon nitride at elevated temperatures generated failures whose kinetics could not be interpreted in terms of static tests. Unloading might play a significant role in extending the time to failure for cyclic fatigue over static fatigue under the same maximum applied stress: it could inhibit development of creep damage or retard accumulation of creep deformation resulting from the relaxation of local stress concentration and recovery of viscoelastic strain. As supported by the microstructural observations, it is likely that the primary failure mechanism for cyclic fatigue at 1260 and 1370 °C might involve the subcritical extension of a localized damage zone originating from the specimen surface where oxidation-assisted damage or oxidation-modified pre-existent flaws would provide favourable sites for crack nucleation. More research of the effects of environments on the fatigue behaviour under various loading modes is necessary.

Acknowledgements

This research was sponsored by the US Department of Energy, Assistant Secretary for Conservation and Renewable Energy, Office of Transportation Technologies, as part of the Ceramic Technology Project of the Materials Development Program, under contract DE-AC05-84OR21400 with Martin Marietta Energy Systems, Inc. C.-K. J. Lin was supported in part by an appointment to the Oak Ridge National Laboratory Postdoctoral Research Program administered by the Oak Ridge Institute for Science and Education. The

authors thanks Drs K. Breder and A. Wereszczak for reviewing the manuscript and for their helpful comments.

References

1. H. E. HELMS, R. A. JOHNSON and L. E. GROSECLOSE, in Proceedings of the Twenty-Third Automotive Technology Development Contractors' Coordination Meeting, P-165 (Society of Automotive Engineers, Warrendale, Pennsylvania, 1986) p. 137.
2. D. CARRUTHERS and L. LINDBERG, in Proceedings of the Third International Symposium on Ceramic Materials and Components for Engines, edited by V. J. Tennery (American Ceramic Society, Westerville, Ohio, 1989) p. 1258.
3. R. KOSSOWSKY, D. G. MILLER and E. S. DIAZ, *J. Mater. Sci.* **10** (1975) 983.
4. G. D. QUINN, *ibid.* **25** (1990) 4361.
5. *Idem, ibid.* **25** (1990) 4377.
6. D. C. CRANMER, B. J. HOCKEY, S. M. WIEDERHORN and R. YECKLEY, *Ceram. Engng Sci. Proc.* **12** (1991) 1862.
7. M. K. FERBER and M. G. JENKINS, *J. Amer. Ceram. Soc.* **75** (1992) 2453.
8. T. FETT, G. HIMSOLT and D. MUNZ, *Adv. Ceram. Mater.* **1** (1986) 179.
9. L. X. HAN and S. SURESH, *J. Amer. Ceram. Soc.* **72** (1989) 1233.
10. L. EWART and S. SURESH, *J. Mater. Sci.* **27** (1992) 5181.
11. C.-K. J. LIN, T. A. MAYER and D. F. SOCIE, in "Cyclic Deformation, Fracture, and Nondestructive Evaluation of Advanced Materials", ASTM STP 1157, edited by M. R. Mitchell and O. Buck (American Society for Testing and Materials, Philadelphia, 1992) p. 3.
12. C.-K. J. LIN and D. F. SOCIE, *J. Amer. Ceram. Soc.* **74** (1991) 1511.
13. C.-K. J. LIN, D. F. SOCIE, Y. XU and A. ZANGVIL, *ibid.* **75** (1992) 637.
14. M. MASUDA, T. SOMA, M. MATSUI and I. ODA, *J. Ceram. Soc. Jpn* **97** (1989) 612.
15. Y. TAJIMA, K. URASHIMA, M. WATANABE and Y. MATSUO, in Proceedings of the Third International Symposium on Ceramic Materials and Components for Engines, edited by V. J. Tennery (American Ceramic Society, Westerville, Ohio, 1989) p. 719.
16. T. OHJI, Y. YAMAUCHI, W. KANEMATSU and S. ITO, *J. Ceram. Soc. Jpn, Int. Edn* **98** (1990) 1070.
17. A. G. EVANS, L. R. RUSSELL and D. W. RICHERSON, *Metall. Trans. A* **6** (1975) 707.
18. M. KAWAI, H. FUJITA, Y. KANKI, H. ABE and J. NAKAYAMA, in Proceedings of the First International Symposium on Ceramic Components for Engines, edited by S. Somiya, E. Kanai and K. Ando (Elsevier, London, 1983) p. 269.
19. L. EWART and S. SURESH, *J. Mater. Sci. Lett.* **22** (1987) 1173.
20. M. J. REECE, F. GUIU and M. F. R. SAMMUR, *J. Amer. Ceram. Soc.* **72** (1989) 348.
21. S. HORIBE, *J. Eur. Ceram. Soc.* **6** (1990) 89.
22. R. H. DAUSKARDT, D. B. MARSHALL and R. O. RITCHIE, *J. Amer. Ceram. Soc.* **73** (1990) 893.
23. C.-K. J. LIN and D. SOCIE, in "Low Cycle Fatigue and Elasto-Plastic Behavior of Materials-3", edited by R.-T. Rie (Elsevier, London, 1992) p. 25.
24. C.-K. J. LIN, M. G. JENKINS and M. K. FERBER, *J. Eur. Ceram. Soc.*, **12** (1993) 3.
25. S. M. WIEDERHORN, in "Fracture Mechanics of Ceramics", Vol. 2, edited by R. C. Bradt, D. P. H. Hasselman and F. F. Lange (Plenum, New York, 1974) p. 623.
26. J. E. RITTER, in "Fracture Mechanics of Ceramics", Vol. 4, edited by R. C. Bradt, D. P. H. Hasselman and F. F. Lange (Plenum, New York, 1978) p. 667.
27. A. G. EVANS and E. R. FULLER, *Metall. Trans. A* **5** (1974) 27.
28. A. VENKATESWARAN, K. Y. DONALDSON and D. P. H. HASSELMAN, *J. Amer. Ceram. Soc.* **71** (1988) 565.
29. D. P. H. HASSELMAN, A. VENKATESWARAN and K. Y. DONALDSON, *J. Mater. Sci.* **24** (1989) 671.
30. S. SURESH and J. R. BROCKENBROUGH, *Acta Metall. Mater.* **38** (1990) 55.
31. M. K. FERBER and M. G. JENKINS, in "Ceramic Technology for Advanced Heat Engines Project", Semiannual Progress Report for October 1991 Through March 1992, ORNL/TM-12133 (Martin Marietta Energy Systems, Inc., Oak Ridge National Laboratory, Oak Ridge, Tennessee, 1992) p. 315.
32. F. C. MONKMAN and N. J. GRANT, *Proc. Amer. Soc. Test. Mater.* **56** (1956) 593.
33. R. W. DAVIDGE, A. G. EVANS, D. GILLING and P. R. WILYMAN, in "Special Ceramics 5", edited by P. Popper (British Ceramic Research Association, Stoke-on-Trent, UK, 1972) p. 329.
34. T. E. EASLER, R. C. BRADT and R. E. TRESSLER, *J. Amer. Ceram. Soc.* **65** (1982) 317.
35. R. RAJ and C. K. CHYUNG, *Acta Metall.* **29** (1981) 159.
36. R. L. TSAI and R. RAJ, *J. Amer. Ceram. Soc.* **65** (1982) C88.
37. D. S. WILKINSON, *ibid.* **71** (1988) 562.
38. S. M. WIEDERHORN, B. J. HOCKEY, D. C. CRANMER and Y. YECKLEY, *J. Mater. Sci.* **28** (1993) 445.
39. B. J. HOCKEY, S. M. WIEDERHORN, W. LIU, J. G. BALDONI and S.-T. BULJAN, *ibid.* **26** (1991) 3931.

Received 7 June
Accepted 13 September 1993